Osteopotentia regulates osteoblast maturation, bone formation, and skeletal integrity in mice

Michael L. Sohaskey,[1,2] Yebin Jiang,[3,4] Jenny J. Zhao,[3,4] Andreas Mohr,[3,5] Frank Roemer,[3,6] and Richard M. Harland[1,2]

[1]Department of Molecular and Cell Biology and [2]Center for Integrative Genomics, University of California, Berkeley, Berkeley, CA 94720
[3]Osteoporosis and Arthritis Research Group, University of California, San Francisco, San Francisco, CA 94117
[4]Osteoporosis and Arthritis Laboratory, Musculoskeletal Division, Department of Radiology, University of Michigan Medical School, Ann Arbor, MI 48109
[5]Department of Radiology, Sligo General Hospital, Sligo, Ireland
[6]Klinikum Augsburg, 86156 Augsburg, Germany

During skeletal development and regeneration, bone-forming osteoblasts respond to high metabolic demand by active expansion of their rough endoplasmic reticulum (rER) and increased synthesis of type I collagen, the predominant bone matrix protein. However, the molecular mechanisms that orchestrate this response are not well understood. We show that insertional mutagenesis of the previously uncharacterized *osteopotentia* (*Opt*) gene disrupts osteoblast function and causes catastrophic defects in postnatal skeletal development. *Opt* encodes a widely expressed rER-localized integral membrane protein containing a conserved SUN (Sad1/Unc-84 homology) domain. Mice lacking Opt develop acute onset skeletal defects that include impaired bone formation and spontaneous fractures. These defects result in part from a cell-autonomous failure of osteoblast maturation and a posttranscriptional decline in type I collagen synthesis, which is concordant with minimal rER expansion. By identifying Opt as a crucial regulator of bone formation in the mouse, our results uncover a novel rER-mediated control point in osteoblast function and implicate human *Opt* as a candidate gene for brittle bone disorders.

Introduction

The skeleton is a highly dynamic organ that remodels and regenerates itself in response to biomechanical stress and physiological trauma. Remodeling and regeneration of bone are made possible by the coordinated activities of its two specialized cell types: osteoblasts, which synthesize and mineralize the bone extracellular matrix, and osteoclasts, which secrete hydrolytic enzymes that resorb this matrix (Karsenty and Wagner, 2002). During embryogenesis and early postnatal development, these activities are uncoupled to enable rapid bone matrix production and growth in response to high metabolic demand, a process termed bone modeling. Accordingly, osteoblasts in prepubertal mice demonstrate a remarkable capacity for bone formation (Hsiao et al., 2008). Despite significant progress in understanding the transcriptional cascades that control skeletogenesis (Karsenty, 2008), the posttranscriptional mechanisms that drive bone modeling are not well understood.

As the predominant protein synthesized by metabolically active osteoblasts, type I collagen accounts for ∼90% of the organic bone matrix (Young, 2003). The production of mature type I collagen is a multistep process that is crucial to a biomechanically stable extracellular matrix. A broad spectrum of genetically and clinically heterogeneous human skeletal dysplasias are caused by mutations in the two type I collagen chains (*COL1A1* and *COL1A2*) or in genes required for collagen processing (Byers and Cole, 2002; Morello et al., 2006; Cabral et al., 2007). Such disorders typically result in low bone mass and include the brittle bone disease osteogenesis imperfecta (OI) and Ehlers-Danlos syndrome. Unfortunately, few existing therapies to correct disorders of low bone mass target de novo bone formation. Thus, it is important to identify new genes

Correspondence to Michael L. Sohaskey: sohaskey@berkeley.edu; or Richard M. Harland: harland@berkeley.edu

Abbreviations used in this paper: μCT, microcomputed tomography; ALP, alkaline phosphatase; Ocn, osteocalcin; OI, osteogenesis imperfecta; Opg, osteoprotegerin; Opt, osteopotentia; PCNA, proliferating cell nuclear antigen; qRT-PCR, quantitative RT-PCR; rER, rough ER; TRAP, tartrate-resistant acid phosphatase; WT, wild type.

The Rockefeller University Press $30.00
J. Cell Biol. Vol. 189 No. 3 511–525
www.jcb.org/cgi/doi/10.1083/jcb.201003006

and molecular networks that regulate osteoblast activity and promote bone formation.

The rough ER (rER) plays a central role in the synthesis and processing of type I collagen (Lamandé and Bateman, 1999; Myllyharju and Kivirikko, 2004). Cotranslational import of type I procollagen into the rER is followed by its posttranslational modification (prolyl and lysyl hydroxylation and glycosylation) and chaperone-mediated folding into a triple-helical conformation. Regulated secretion and extracellular cleavage of the proprotein triple helix then enable its self-assembly into mature fibrils, which are covalently cross-linked and subsequently mineralized to give the bone its characteristic rigidity and toughness. In highly secretory cell types such as osteoblasts and pancreatic islet and acinar cells, the rER undergoes active membrane expansion, greatly increasing its surface area to meet the metabolic demands of the cell (Vedrenne and Hauri, 2006). Precisely how the osteoblast translates the metabolic demand for new bone matrix into tightly coordinated rER expansion and increased type I collagen production, however, is not clear.

In this study, we identify osteopotentia (Opt), a previously uncharacterized rER integral membrane protein, as an essential regulator of postnatal osteoblast maturation. Loss of Opt leads to impaired type I collagen synthesis and a consequent failure of bone modeling. Our results establish a critical role for Opt in osteoblastic bone formation and suggest that mutations in human *Opt* may cause OI and other degenerative bone disorders.

Results

Insertional mutagenesis of Opt, a widely expressed SUN domain protein

In an insertional mutagenesis screen for genes encoding developmentally important secreted and transmembrane proteins (Mitchell et al., 2001), mutagenesis of the uncharacterized gene AI848100 yielded a severe skeletal phenotype; thus, we named this gene *osteopotentia*, or *Opt*. The *Opt* locus comprises 24 exons and encodes a predicted protein of ∼140 kD, having a signal peptide sequence at its N terminus and a single putative transmembrane domain near its C terminus (Fig. 1 A). The protein also contains a highly conserved SUN (Sad1/UNC-84 homology) domain of 130 residues in the amino-terminal half of the protein. SUN domain proteins, including the mammalian inner nuclear membrane proteins SUN1 and SUN2, dictate nuclear positioning and centromere tethering by physically linking the nucleus and cytoskeleton (Tzur et al., 2006; Ding et al., 2007; King et al., 2008; Chi et al., 2009; Razafsky and Hodzic, 2009). No other mouse protein shares extensive sequence similarity with Opt, and genomic database searches identified single *Opt* orthologues in humans, frogs, zebrafish, fruit flies, nematodes, and yeast.

Insertion of the gene trap vector into the 1,624-bp 11th intron of the *Opt* locus produces a fusion between the amino-terminal 424 amino acids of the Opt protein and a transmembrane βgeo reporter (Fig. 1 A). Neither full-length mRNA transcripts nor any transcript spanning the insertion site was detected in mice homozygous for the insertion (Fig. 1, B and C). Endogenous Opt protein migrated as a doublet of ∼260 kD, and

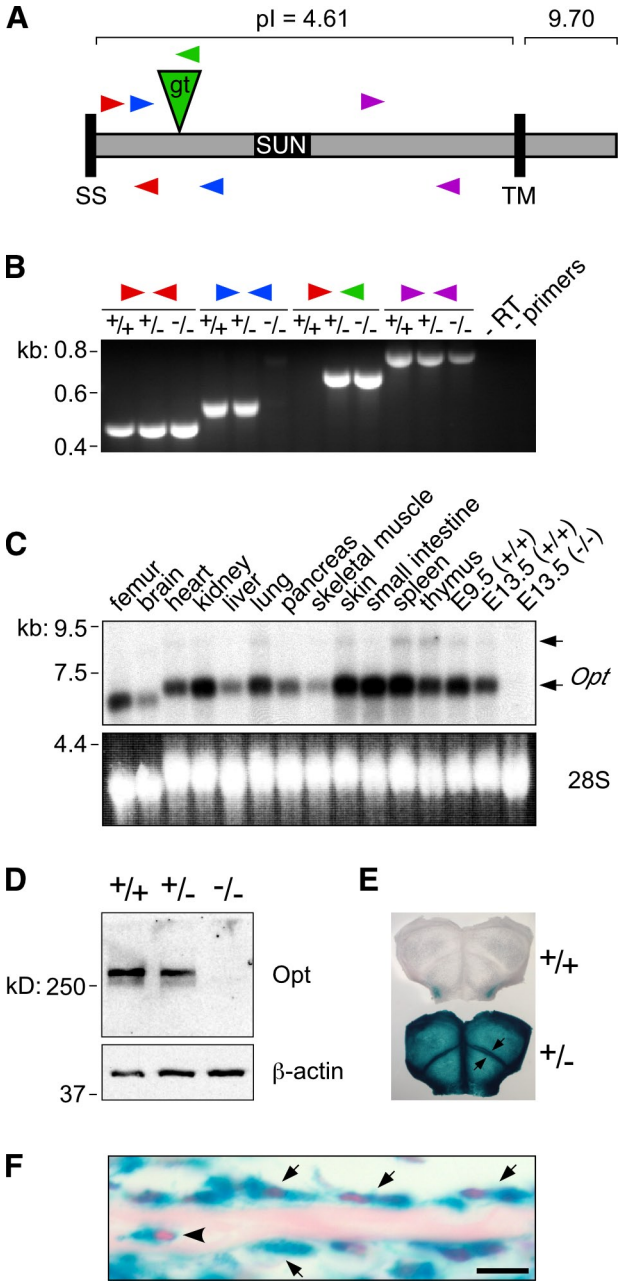

Figure 1. **Identification, mutagenesis, and expression pattern of *Opt*.** (A) Schematic of Opt protein domain organization, showing the position and orientation of the gene trap insertion (gt; green triangle) and RT-PCR primer–binding sites (arrowheads). The positions of the insertion and primer sites relative to the protein are shown primarily for illustrative purposes and are not drawn precisely to scale. SS, signal sequence; TM, putative transmembrane domain; pI, isoelectric point. (B) RT-PCR analysis of E13.5 embryos, confirming that *Opt* transcripts spanning the insertion site (blue arrowheads) are not detected in $Opt^{-/-}$ mice. Primers are shown as in A. +/+, WT; +/−, $Opt^{+/-}$; −/−, $Opt^{-/-}$. (C) Widespread *Opt* expression demonstrated by Northern blot analysis of tissue samples from 10-d-old mice and whole E9.5 and E13.5 embryos. Arrows indicate two specific transcripts (∼7.0 and 9.0 kb) that are absent from the E13.5 $Opt^{-/-}$ sample. 28S, EtBr-stained 28S ribosomal RNA. (D) Immunoblotting of E13.5 whole embryo lysates with Opt (top) or β-actin (bottom) antibodies. (E and F) Opt protein expression visualized as β-galactosidase staining in whole mount (E) and histological sections (F) of newborn calvaria. (E) Arrows indicate strong β-galactosidase staining at osteogenic fronts. (F) Arrows indicate Opt-expressing osteoblasts lining the bone surface, whereas the arrowhead indicates osteocyte expression. Bar, 10 µm.

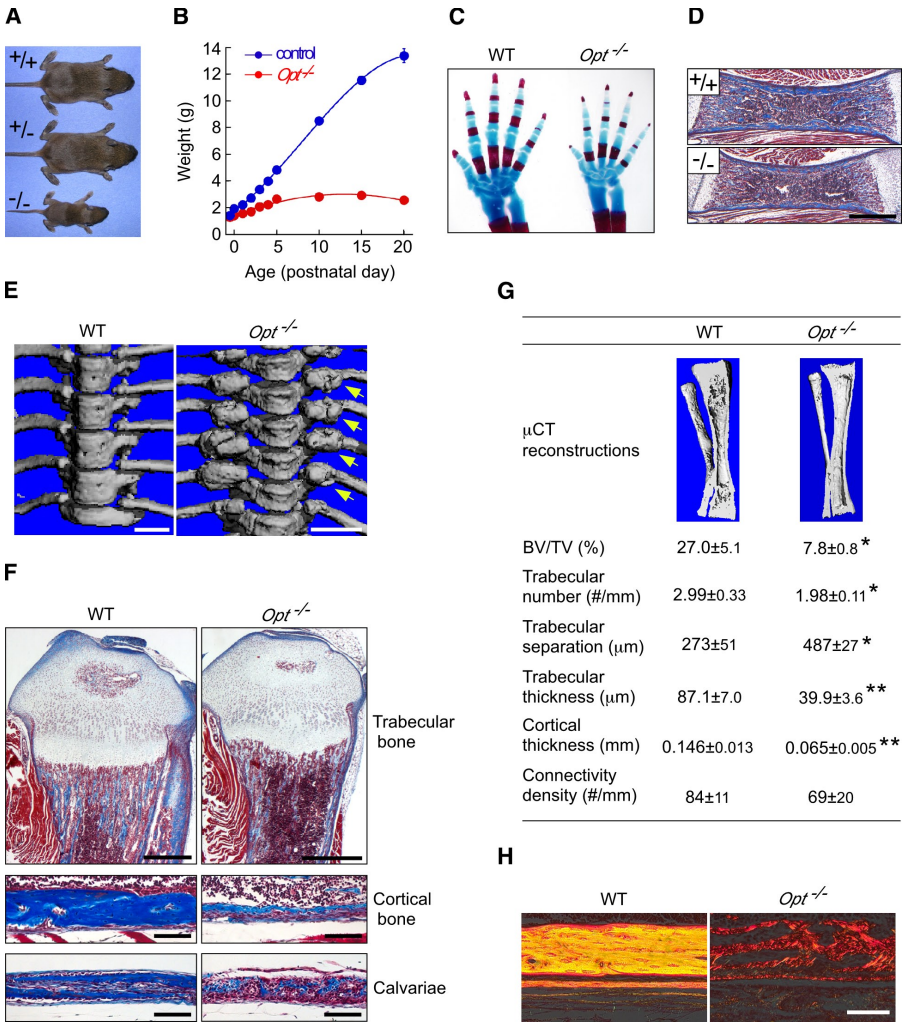

Figure 2. **Growth retardation and low bone mass with multiple fractures in *Opt*$^{-/-}$ mice.** (A) Gross morphology of WT, *Opt*$^{+/-}$, and *Opt*$^{-/-}$ mice at P10. (B) Growth curves for control (WT and *Opt*$^{+/-}$) and *Opt*$^{-/-}$ mice from E18.5 to P20. $P < 0.0001$ for all time points. (C) Cleared skeletal preparations of neonatal forelimbs stained with Alcian blue for cartilage and Alizarin red for bone. Note the delayed ossification of metacarpals and phalanges in the *Opt*$^{-/-}$ autopod. The mutant forelimb was digitally cut and moved within the same image using Photoshop to align it with and position it in closer proximity to the WT forelimb. (D) Longitudinal sections from P0 femurs stained with Masson's trichrome to visualize collagen (blue) and muscle (red). Bar, 0.5 mm. (E) μCT reconstructions showing hyperplastic fracture calluses (arrows) at the costovertebral articulations of *Opt*$^{-/-}$ mice (P20). Bars, 1 mm. (F) Longitudinal sections from P10 tibiae (top and middle) and calvaria (bottom) stained with Masson's trichrome. Bars: (top) 0.5 mm; (middle and bottom) 0.1 mm. (G) μCT reconstructions and bone structural parameters measured by quantitative μCT ($n = 5$). *, $P < 0.05$; **, $P < 0.01$. (H) Polarization microscopy of Sirius red–stained collagen fibers, showing abnormal birefringence of *Opt*$^{-/-}$ cortical bone. Bar, 0.1 mm.

expression of both bands was negligible in homozygous mutant embryos (Fig. 1 D). Importantly, we did not detect smaller molecular mass bands on Opt immunoblots, indicating that no stable protein product was synthesized from potential alternatively spliced mutant transcripts (Fig. 1 B, purple arrowheads). Moreover, the βgeo fusion protein is unlikely to retain any Opt activity, as "secretory trap" products typically accumulate in cytoplasmic inclusion bodies (Skarnes et al., 1995; Mitchell et al., 2001). Collectively, these results suggest that the *Opt* gene trap insertion generates a null or strongly hypomorphic allele.

Opt mRNA and protein are widely expressed during embryogenesis and early postnatal life (Fig. 1, C, E, and F). β-Galactosidase activity was detected in all skeletal elements, as demonstrated by whole mount X-gal staining of newborn calvaria in which prominent staining was evident at osteogenic fronts (Fig. 1 E, arrows). In histological sections, β-galactosidase activity was apparent in chondrocytes as well as in osteoblasts, osteoclasts, and osteocytes (Fig. 1 F and not depicted).

Mice lacking Opt exhibit catastrophic defects in bone modeling

Heterozygous (*Opt*$^{+/-}$) mice were viable, fertile, and phenotypically indistinguishable from wild-type (WT) littermates. In contrast, most homozygous (*Opt*$^{-/-}$) mice died neonatally; this number was ~50% on a mixed C57BL6/CD1 genetic background and 100% on an inbred C57BL6/129Ola background. For this reason, animals on a mixed C57BL6/CD1 background were used for all subsequent experiments. Neonatal *Opt*$^{-/-}$ mice frequently showed labored breathing and died after failing to acquire the healthy pink hue of their control littermates; the smaller size of the mutant ribcage (Fig. S1) may account for this respiratory distress and neonatal lethality. *Opt*$^{-/-}$ mice that survived this perinatal crisis nonetheless failed to thrive and showed significantly reduced body weights as early as embryonic day (E) 18.5 (Fig. 2, A and B). Consistent with normal nutrition, surviving *Opt*$^{-/-}$ mice frequently showed a conspicuous milk spot in their stomachs and had a normal percentage of body fat as assessed by dual-energy x-ray absorptiometry (unpublished data). However, mutant animals displayed an imbalanced gait and an impaired righting response, which is suggestive of potential neurological defects. Mortality among surviving *Opt*$^{-/-}$ mice was >80% by postnatal day (P) 10, and none survived to weaning.

Skeletal development was modestly delayed in neonatal *Opt*$^{-/-}$ mice (Fig. 2 C and Fig. S1), with mutant long bones having less trabecular and cortical bone than WT (Fig. 2 D). Beginning at ~P5, *Opt*$^{-/-}$ mice exhibited striking skeletal deformities

Table I. **Serum parameters in 5-d-old mice**

Parameter	WT	*Opt*$^{+/-}$	*Opt*$^{-/-}$	*n*
Calcium (mg/dl)	4.9 ± 0.5	5.0 ± 0.3	5.2 ± 0.5	10
Phosphate (mg/dl)	16.3 ± 0.4	16.3 ± 0.5	17.4 ± 0.7	10
ALP (U/liter)	514 ± 44.7	458 ± 21.9	737 ± 78.3[b]	10
IGF-1 (ng/ml)	132 ± 18.3	131 ± 8.48	68.4 ± 11.0[b]	9–10
PTH (pg/ml)	49.6 ± 13.2	45.0 ± 6.64	47.6 ± 11.8	13–17
Ascorbic acid (μM)	103 ± 4.22	126 ± 6.39[a]	115 ± 5.59	12

PTH, parathyroid hormone. Data are expressed as mean ± SEM.
[a]$P < 0.05$.
[b]$P < 0.01$.

that included misshapen long bones, internal hemorrhaging around forelimbs and cervical vertebrae, inflexible joints, and spontaneous fractures. Hyperplastic calluses formed throughout the *Opt*$^{-/-}$ axial and appendicular skeleton, which is suggestive of aberrant ongoing fracture repair (Fig. 2 E). In addition, the cranial vault of *Opt*$^{-/-}$ mice was flatter than that of control littermates, with widened sutures (unpublished data). Histology and quantitative microcomputed tomography (μCT) revealed significantly reduced trabecular bone volume and dramatically thinner cortices in long bones from P10 *Opt*$^{-/-}$ mice, despite only mild perturbations to the organization of growth plate chondrocytes (Fig. 2 F). Trabecular number and thickness decreased significantly in *Opt*$^{-/-}$ long bones, whereas trabecular separation increased (Fig. 2 G). Consistent with these findings, *Opt*$^{-/-}$ cortical bone resembled immature woven bone with sparse and randomly oriented type I collagen fibrils, which is in contrast to the birefringent, lamellar organization of WT bone (Fig. 2 H). Mutant calvarial bones also showed marked thinning (Fig. 2 F), confirming that Opt deficiency affects both endochondral and intramembranous ossification.

We measured biochemical indices of bone turnover to assess whether metabolic abnormalities contribute to the *Opt*$^{-/-}$ brittle bone phenotype (Table I). Serum calcium, phosphate, and parathyroid hormone levels were unchanged, whereas a decrease in circulating IGF-1 may explain in part the poor growth of *Opt*$^{-/-}$ mice (Baker et al., 1993; Rosen, 2004). Elevated alkaline phosphatase (ALP), a condition associated with fracture callus formation (Glorieux et al., 2000), was also seen in *Opt*$^{-/-}$ animals. Defective ascorbate synthesis has been shown to induce fractures in young mice (Mohan et al., 2005); however, serum ascorbate levels were normal in the absence of Opt. Moreover, hypoglycemia without hyperinsulinemia (Fig. S4 A) excluded a dysregulation of energy metabolism as the underlying cause of the *Opt*$^{-/-}$ skeletal phenotype. Collectively, these data indicate that Opt deficiency causes a generalized, rapid onset impairment of bone modeling, leading to spontaneous fractures in neonatal mice.

Opt is required postnatally for terminal osteoblast differentiation

The low bone mass and fracture-prone nature of young *Opt*$^{-/-}$ mice suggested a failure of postnatal osteoblast function. Consistent with this hypothesis, serum protein levels of osteocalcin, the definitive marker of mature osteoblasts, decreased to 43% and 18% of controls by P5 and P10, respectively (Fig. 3 A). Quantitative RT-PCR (qRT-PCR) confirmed a marked reduction in *osteocalcin* (*Ocn*) transcripts in long bone samples from P10 *Opt*$^{-/-}$ mice, along with significant reductions in *Alp*, *Bsp* (bone sialoprotein), and the prodifferentiation VEGF receptor *Flk1*, as well as *Col1a1* and *Col1a2*, encoding the two type I procollagen chains (Fig. 3 B). Importantly, expression of the osteoblast-restricted transcription factors *Atf4* (activating transcription factor 4), *Runx2* (runt-related transcription factor 2), and *osterix* was comparable in WT and *Opt*$^{-/-}$ samples, suggesting that Opt is dispensable for commitment to the osteoblast lineage. These qRT-PCR data were verified by in situ hybridization, with *Ocn* transcripts in particular being nearly undetectable in *Opt*$^{-/-}$ bones (Fig. 3 C). Thus, Opt is crucial for postnatal osteoblast maturation. Intriguingly, neither von Kossa staining nor osteoblast marker expression was consistently altered in E17.5 mutant femurs (Fig. S2 B). Collectively with our finding of delayed ossification in neonatal *Opt*$^{-/-}$ mice (Fig. 2, C and D), these results indicate that Opt is initially required for proper bone modeling during late embryogenesis. Moreover, Opt is dispensable for chondrogenesis, as chondrocyte organization and maturation appeared normal in E14.5 *Opt*$^{-/-}$ long bones (Fig. S2 A).

The nominal amount of secondary spongiosa and abnormal osteoblast morphology in *Opt*$^{-/-}$ bones (see Fig. 4 A and Fig. 7 A) precluded static histomorphometry of osteoblast parameters. Similarly, attempts to quantify bone formation rates after in vivo labeling with calcein, a fluorescent indicator of newly formed bone, yielded punctate, discontinuous labeling of mutant bone surfaces that contrasted sharply with the regular labeling of WT surfaces (Fig. 3 D). This is consistent with decreased osteoblast marker expression and with the woven appearance of *Opt*$^{-/-}$ bone (Fig. 2 H). Nonetheless, the osteoid that did form throughout the *Opt*$^{-/-}$ skeleton appeared properly mineralized (Fig. 3 E), suggesting that loss of Opt does not cause rickets.

To address whether decreased proliferation or increased cell death contributes to the *Opt* phenotype, we analyzed cortical bone sections by proliferating cell nuclear antigen (PCNA) immunohistochemistry and TUNEL staining. A slight though insignificant increase in the percentage of PCNA-positive *Opt*$^{-/-}$ osteoblasts (Fig. 3 F) indicated that reduced cell proliferation is not responsible for the low bone mass. In contrast, apoptosis assayed by TUNEL increased from 0.8% in WT bones to 1.9% in mutants (Fig. 3 G). Given that apoptotic rates for WT mouse osteoblasts in vivo typically fall in the range of 1–2%

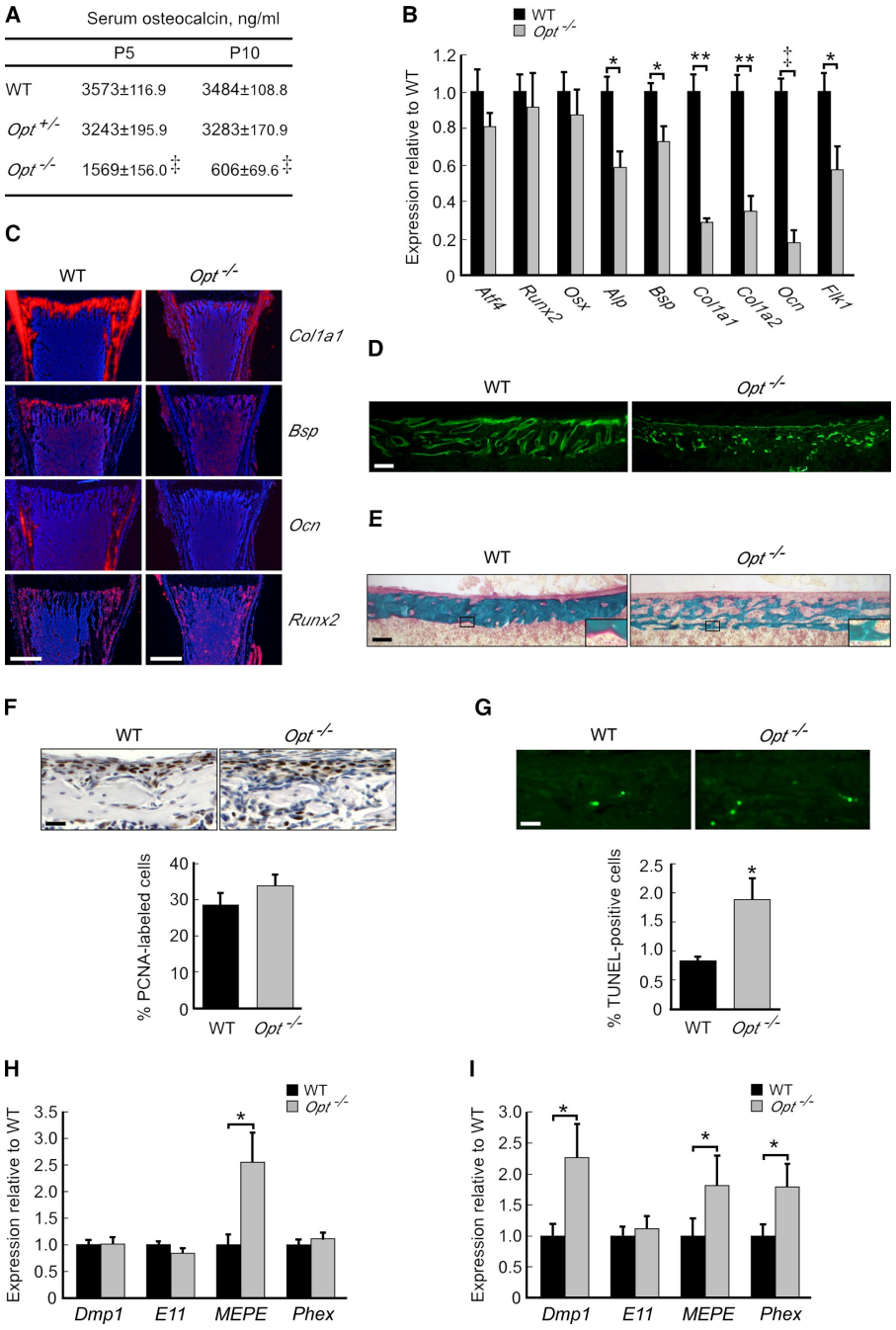

Figure 3. **Impaired osteoblast maturation in *Opt*$^{-/-}$ mice.** (A) Serum osteocalcin levels expressed as ng/ml (n = 12). (B) qRT-PCR of osteoblast markers in femurs from P10 mice (n = 4). (C) Radioactive in situ hybridization on serial sections from distal femurs (P10). Bars, 0.5 mm. (D) Irregular calcein labeling of cortical bone surfaces in *Opt*$^{-/-}$ femurs (P10). (D–G) Bars, 0.1 mm. (E) Goldner's trichrome staining of cortical bone in undecalcified femur sections (P10). Higher magnification insets of the boxed regions show decreased osteoid production (pink) by *Opt*$^{-/-}$ osteoblasts. (F and G) PCNA immunohistochemistry (F) and TUNEL analysis (G) of cortical bone from P3 femurs. Data are expressed as PCNA-positive (brown) or TUNEL-positive (green) cells per total cell number (n = 5–6 mice/genotype). (H and I) qRT-PCR of osteocyte markers in femurs (H) and calvaria (I) from P10 mice. *, $P < 0.05$; **, $P < 0.01$; ‡, $P < 0.0001$. Error bars indicate SEM.

(Jilka et al., 1999), this modest 1% increase in cell death is likely a secondary effect of Opt deficiency rather than the primary cause of the observed defects.

Increased numbers of terminally differentiated osteocytes have been reported in association with immature woven bone (Noble and Reeve, 2000; Hernandez et al., 2004); thus, we quantified osteocyte differentiation markers in WT and *Opt*$^{-/-}$ bones. Consistent with increased osteocyte numbers, expression of *MEPE* (*matrix extracellular phosphoglycoprotein*) was significantly up-regulated in *Opt*$^{-/-}$ calvaria and femurs, whereas *Dmp1* (*dentin matrix protein 1*) and *Phex* (*phosphate-regulating gene with homologies to endopeptidases on the x chromosome*) were also up-regulated in mutant calvaria. These data indicate an increase in osteocyte numbers associated with the immature woven bone that is prevalent in the *Opt*$^{-/-}$ skeleton.

To further assess the consequences of Opt inactivation in vivo, we analyzed osteoblast maturation during fracture repair in postnatal *Opt*$^{-/-}$ mice. Hyperplastic calluses from P12 (Fig. 4) and P15 (not depicted) ribs and long bones consisted largely of calcified cartilage associated with *Col2a1*-expressing chondrocytes (Fig. 4, A and C), which is consistent with the reported progression of repair in nonstabilized fractures (Thompson et al., 2002; Colnot et al., 2003; Behonick et al., 2007). Strikingly, small, immature *Col1a1*-expressing osteoblasts were also evident throughout the callus and fracture site (Fig. 4, A [insets] and D). Time course studies of nonstabilized fracture repair have

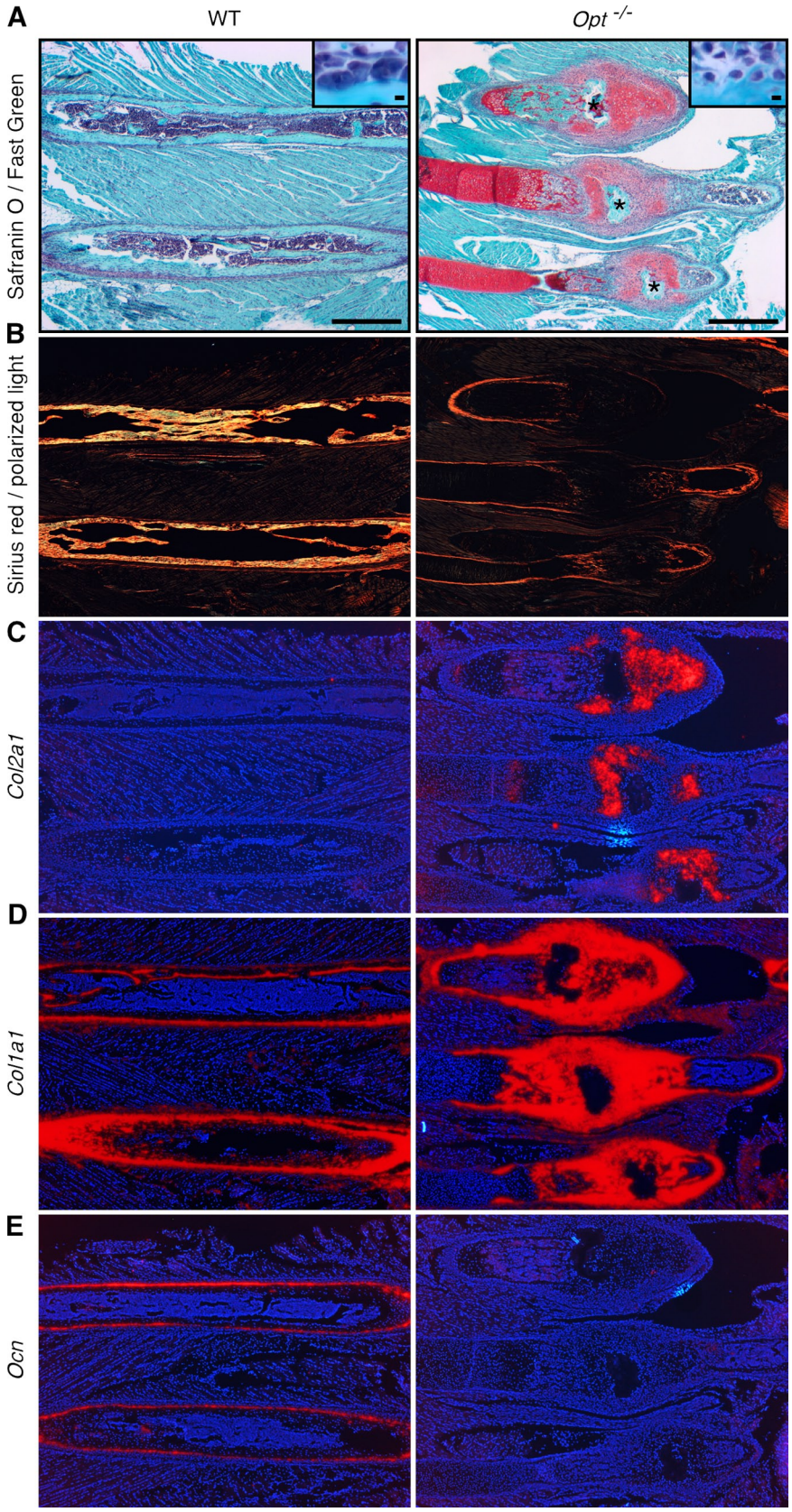

Figure 4. **Hyperplastic fracture calluses in *Opt*$^{-/-}$ mice lack mature osteoblasts.** Images show serial sections of three hyperplastic rib calluses (*Opt*$^{-/-}$) or two corresponding intact ribs (WT) from P12 mice. (A) Safranin O/Fast green staining with hematoxylin counterstain. Central fracture sites are indicated by asterisks. Higher magnification insets show enlarged active osteoblasts lining the WT bone compared with smaller immature osteoblasts seen in mutant fracture calluses. Bars: (main images) 1 mm; (insets) 10 µm. (B) Polarization microscopy of Sirius red–stained collagen fibers, showing minimal woven bone formation in *Opt*$^{-/-}$ calluses. (C–E) Radioactive in situ hybridization for *Col2a1* (C), *Col1a1* (D), and *Ocn* (E). Note the robust *Col1a1* expression but negligible *Ocn* expression in *Opt*$^{-/-}$ calluses.

reported *Ocn* expression in presumptive perichondrial cells before the callus remodeling stage (Ferguson et al. 1999; Thompson et al. 2002); however, mature *Ocn*-expressing osteoblasts and newly formed bone were undetectable in *Opt*$^{-/-}$ fractures (Fig. 4, B and E). Thus, although a time course study of bone repair in spontaneous fractures is precluded, our analysis indicates that

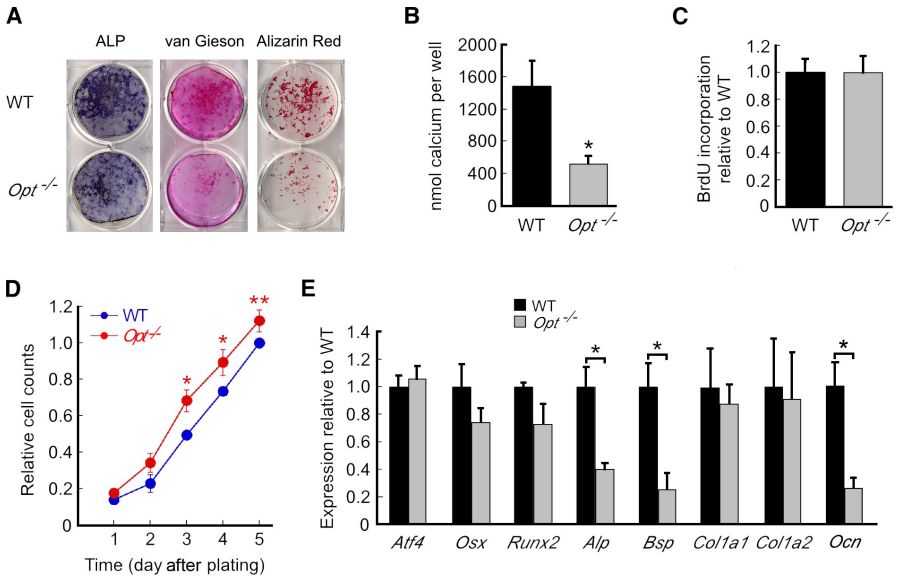

Figure 5. **Defective matrix deposition and bone formation by *Opt*$^{-/-}$ osteoblasts.** (A) Primary calvarial osteoblasts were plated at equal densities and were grown to confluence before switching to mineralization media on day 0. Cultures were assayed for ALP activity or stained with van Gieson reagent (to stain collagen fibrils) on day 10, and bone nodules were visualized by Alizarin red staining on day 14. (B) Bone formation quantified as eluted Alizarin red stain (n = 5 independent experiments in triplicate). (C) BrdU incorporation by proliferating osteoblasts assayed on day 5 after plating. (D) Growth curves for WT and *Opt*$^{-/-}$ osteoblasts over 5 d (n = 3 independent experiments in triplicate). (E) qRT-PCR analysis of primary osteoblasts on day 7 of differentiation. *, P < 0.05; **, P < 0.01. Error bars indicate SEM.

activated osteoblasts at the fracture site robustly express *Col1a1* but fail to express *Ocn*. Robust *Col1a1* expression in turn implies that decreased *Col1a1*/*Col1a2* expression in intact P10 bones (Fig. 3 B) may result secondarily from the marked disruption of osteoblast maturation and bone formation in *Opt*$^{-/-}$ mice (see Discussion).

To determine the cellular basis for the skeletal defects in *Opt*$^{-/-}$ mutants, we compared the differentiation capacity and bone-forming potential of primary calvarial osteoblasts from WT and *Opt*$^{-/-}$ mice. Consistent with in vivo data, *Opt*$^{-/-}$ osteoblast cultures showed reduced ALP activity, a sparsely formed collagen matrix, and significantly fewer bone nodules than WT cultures after 2 wk in differentiation media (Fig. 5, A and B). These defects were not the result of compromised cell matrix adhesion and consequent cell death, as WT and mutant osteoblasts adhered equally well to a fibronectin or type I collagen substratum (Fig. S3). Likewise, BrdU incorporation was similar for WT and *Opt*$^{-/-}$ osteoblasts (Fig. 5 C), again arguing that reduced cell proliferation does not account for the aberrant differentiation of mutant osteoprogenitors. Indeed, when plated at the same density as WT osteoblasts, *Opt*$^{-/-}$ osteoblasts grew at a faster rate, resulting in increased cell numbers over a 5-d culture period (Fig. 5 D).

Decreased differentiation potential was confirmed by reduced expression of *Alp*, *Bsp*, and *Ocn* in differentiating *Opt*$^{-/-}$ osteoblasts; in contrast, expression of the transcription factors *Atf4*, *Runx2*, and *Osterix* remained largely unchanged (Fig. 5 E). Thus, like their counterparts in vivo, primary *Opt*$^{-/-}$ osteoblasts differentiated poorly and showed functional defects in type I collagen matrix deposition and bone formation. These findings indicate that the brittle bone phenotype of *Opt*$^{-/-}$ mice results, at least in part, from failed postnatal bone formation secondary to a cell-autonomous impairment of osteoblast maturation.

Compromised osteoclast function reveals a state of low bone turnover in *Opt*$^{-/-}$ mice

Because increased bone resorption may exacerbate the low bone mass of *Opt*$^{-/-}$ mice (Karsenty and Wagner, 2002), we next assessed osteoclast function by qRT-PCR, clinical chemistry, and histomorphometric analyses. Expression of several osteoclast transcripts, including β3-integrin, calcitonin receptor, cathepsin K, and tartrate-resistant acid phosphatase (TRAP), was moderately or significantly reduced in *Opt*$^{-/-}$ femurs and calvaria (Fig. 6, A and B). Likewise, decreased levels of osteoclast-specific TRAP enzymatic activity were found in the serum and long bones of *Opt*$^{-/-}$ mice (Fig. 6 C), and mutant animals excreted significantly fewer urinary deoxypyridinoline cross-links (a specific indicator of bone resorption resulting from type I collagen breakdown; Fig. 6 D). Osteoclast numbers were also significantly reduced in mutant femurs (Fig. 6 E).

Osteoblasts regulate osteoclastogenesis through the production of cytokines, including the proosteoclastogenic factor *Rankl* (receptor activator of nuclear factor-κB ligand) and the antiosteoclastogenic decoy receptor *osteoprotegerin* (*Opg*). The *Rankl*/*Opg* ratio is a key determinant of the extent of osteoclastogenesis (Boyle et al., 2003). In long bones and calvaria from *Opt*$^{-/-}$ mice, the ratio of *Rankl* to *Opg* expression was reduced by ∼50% (Fig. 6 F), suggesting that diminished osteoclast function results at least in part from aberrant osteoblast signaling. Collectively with our osteoblast data, these findings indicate that Opt deficiency creates a physiological imbalance in which decreased bone resorption accompanies a more severe reduction in bone formation.

Opt promotes the synthesis of type I collagen by metabolically active osteoblasts

Our qRT-PCR results revealed comparable *Col1a1* and *Col1a2* expression by cultured WT and *Opt*$^{-/-}$ osteoblasts (Fig. 5 E) despite the relatively sparse collagen matrix deposited by mutant osteoblast cultures (Fig. 5 A, middle). This apparent discrepancy suggested that Opt is required for the synthesis and/or secretion of type I collagen protein by metabolically active osteoblasts. Consistent with impaired protein synthesis, *Opt*$^{-/-}$ osteoblasts were smaller than their WT counterparts in vivo (Fig. 7 A). In contrast, bone marrow stromal cells from WT and

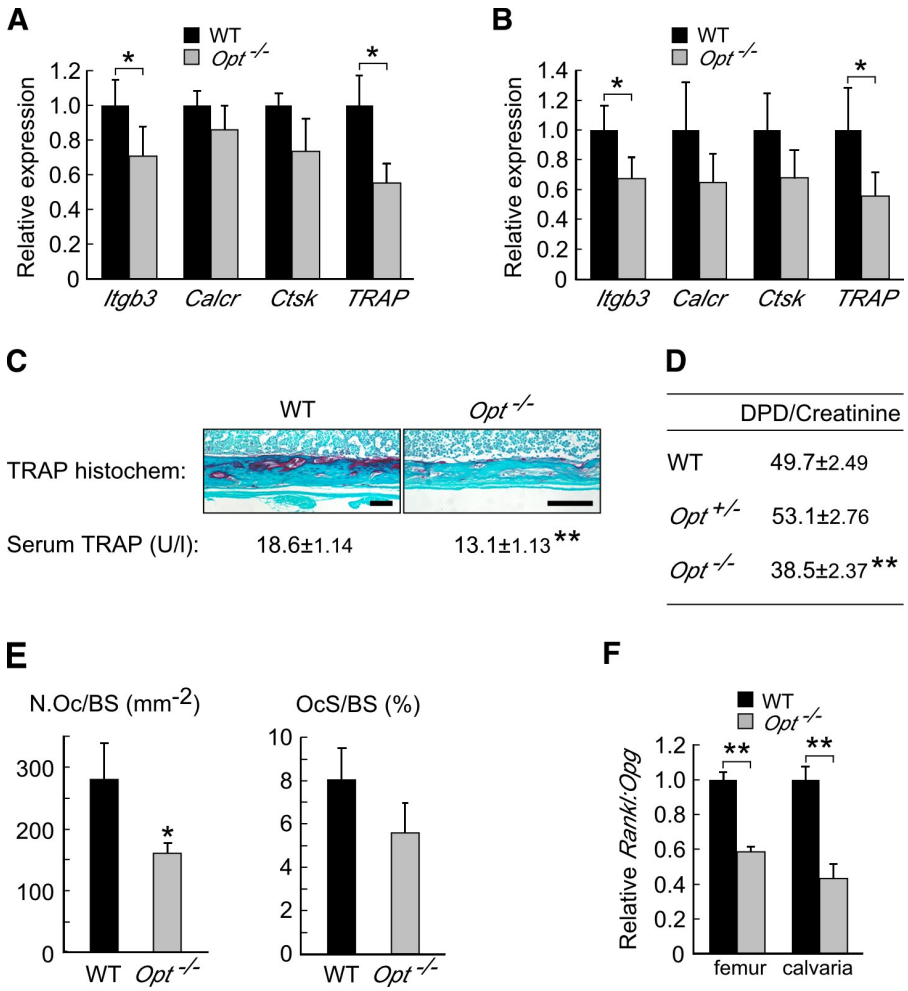

Figure 6. ***Opt*$^{-/-}$ mice exhibit diminished osteoclast function.** (A and B) qRT-PCR of osteoclast markers in femurs (A; $n = 4$) and calvaria (B; $n = 5$) from P10 mice. (C) Decreased osteoclast-specific TRAP activity in *Opt*$^{-/-}$ bones assayed by histochemical staining (P10 tibial sections) and serum ELISA (P5 mice). Bars, 0.1 mm. (D) Urinary deoxypyridinoline (DPD) cross-links from P5 mice ($n = 9$–10). (E) Osteoclast number/bone surface (N.Oc/BS) and osteoclast surface/bone surface (OcS/BS) in femurs from P10 mice ($n = 5$). (F) Reduced ratio of *Rankl* to *Opg* expression in *Opt*$^{-/-}$ femurs and calvaria assessed by qRT-PCR. *, $P < 0.05$; **, $P < 0.001$.

Opt$^{-/-}$ mice were similar in size, again suggesting that Opt deficiency is particularly detrimental to committed osteoblasts. Ultrastructural analyses also supported a defect in protein synthesis in mutant osteoblasts. Strikingly, although WT osteoblasts demonstrated the extensive, well-organized rER characteristic of metabolically active cells, *Opt*$^{-/-}$ osteoblasts adopted a fibroblastic appearance with a scarce, discontinuous rER network and a higher nuclear/cytoplasmic ratio (Fig. 7 B). Consistent with the modest delay in bone formation seen in neonatal mice (Fig. 2, C and D), similar though less-pronounced ultrastructural defects were observed in osteoblasts from E17.5 *Opt*$^{-/-}$ long bones (Fig. S2 C).

To directly test the hypothesis that Opt is crucial for type I collagen synthesis in mature osteoblasts, we metabolically labeled proliferating (5 d after plating) and confluent differentiating (12 d after plating) osteoblast cultures for 12 h in media containing nonessential amino acids and quantified the resulting radiolabeled collagen (Fig. 7 C). When normalized to β-actin protein levels, no significant difference was measured in the amount of type I collagen synthesized by proliferating WT and *Opt*$^{-/-}$ osteoblasts (Fig. 7 E). Notably, absolute levels of both type I collagen and β-actin were increased in proliferating *Opt*$^{-/-}$ cultures (Fig. 7 D), which is consistent with the faster growth rate of mutant cells (Fig. 5 D). In contrast, differentiating *Opt*$^{-/-}$ osteoblasts showed a 35–80% reduction in their synthesis of both type I collagen chains, despite a modest (~15%) reduction in β-actin levels (Fig. 7, D and E) and comparable gene expression of *Col1a1* and *Col1a2* (Fig. 7 F). Delayed electrophoretic migration of collagen chains from mutant cells suggested their overmodification (Fig. 7, D and G); however, no change in hydroxylation (prolyl 3, prolyl 4, or lysyl) was detected by tandem mass spectrometry (not depicted). Importantly, decreased collagen levels were not caused by impaired secretion and intracellular retention of procollagen, as type I procollagen assessed by immunoblotting was similarly reduced in *Opt*$^{-/-}$ osteoblast lysates (Fig. 7 D, Pro-α1(I)) as well as in mutant long bones and calvaria (not depicted). In addition, steady-state expression of the ER-resident proteins GRP78/BiP, GRP94, and calnexin was unchanged in mutant osteoblasts (Fig. 7 H), indicating that the decreased synthesis seen for type I collagen did not broadly affect secretory pathway proteins.

To further establish whether loss of Opt causes a generalized defect in protein synthesis, we examined the pancreas, another organ adapted to robust protein synthesis and secretion. Neither endocrine nor exocrine pancreatic function or ultrastructure was altered by Opt deficiency (Fig. S4), as mutant acini contained abundant zymogen granules and extensive rER surface area, unlike the sparse rER of mutant osteoblasts. Moreover,

aside from modest glomerular hypercellularity in the kidneys, no gross histological changes were detected in other major organs from *Opt*$^{-/-}$ mice (unpublished data). These data suggest that Opt is dispensable for normal pancreatic function in young mice and argue that, despite its widespread expression, impaired protein synthesis is not an inevitable consequence of Opt deficiency in nonskeletal tissues. In contrast, the metabolic demands of perinatal bone formation reveal that Opt is a critical regulator of type I collagen synthesis in osteoblasts.

Opt is a glycosylated transmembrane protein of the rER

Based on the disrupted ER ultrastructure and decreased type I collagen synthesis in *Opt*$^{-/-}$ osteoblasts, we tested the hypothesis that *Opt* encodes an ER-localized protein. When overexpressed in primary osteoblasts or established cell lines, epitope-tagged full-length Opt showed extensive colocalization with the general ER markers calnexin and protein disulfide isomerase but limited colocalization with the Golgi markers TGN46 and GM130 (Fig. 8 A and not depicted). ER localization was not disrupted by deletion of the SUN domain (Fig. 8 A, bottom) or by treatment with brefeldin A, a fungal metabolite that causes Golgi disassembly (unpublished data). Our attempts to detect endogenous Opt by indirect immunofluorescence were unsuccessful; thus, we fractionated WT mouse embryonic fibroblast lysates by continuous density gradient ultracentrifugation and analyzed fractions by immunoblotting. Endogenous Opt cofractionated with ER markers but showed no overlap with markers of the Golgi or plasma membrane (Fig. 8 B). Notably, Opt fractionated most precisely with ribophorin I, a ribosomal binding protein that localizes specifically to the rER (Kreibich et al., 1978).

N-glycosylation status can also be used to track a protein's position in the secretory pathway, and Opt contains 11 potential N-glycosylation sites in its predicted luminal domain. Before transiting from the ER to the Golgi, N-linked carbohydrates are sensitive to hydrolysis by the glycosidase Endo H; subsequently, they become resistant to Endo H while gaining sensitivity to the glycosidase PNGase F. Like the well-characterized ER luminal protein GRP94, Opt demonstrated sensitivity to both Endo H and PNGase F (Fig. 8 C). In contrast, the Golgi-resident protein JAWS/gPAPP (Frederick et al., 2008; Sohaskey et al., 2008) showed sensitivity to PNGase F but not Endo H. We conclude that Opt is an N-glycosylated rER-resident protein.

Fractionating lysates into membrane and cytosolic compartments revealed that Opt, like the ER integral membrane protein calnexin, partitions exclusively into the membrane fraction (Fig. 8 D). Treatment of membranes with high salt or alkaline pH failed to release Opt into the soluble fraction, whereas treatment with detergent solubilized most of the membrane-associated calnexin but only a limited portion of the Opt (Fig. 8 E). Moreover, Opt partitioned into the detergent phase during Triton X-114 phase separation (unpublished data), confirming its membrane localization and excluding the possibility that the protein is sequestered in the ER lumen. Collectively, these findings identify Opt as a glycosylated integral membrane protein of the rER, with its amino-terminal SUN domain exposed to the rER lumen (Fig. 8 F).

Discussion

The molecular mechanisms underlying the osteoblastic response to high metabolic demand during perinatal bone modeling are not well understood. In this study, we report that Opt, a newly identified integral membrane protein of the rER, plays an essential role in promoting type I collagen synthesis, rER expansion, and terminal osteoblast differentiation. Our results implicate Opt as a crucial determinant of bone mass in mice and suggest that its inactivation may likewise lead to metabolic bone disease in humans.

The most conspicuous feature of the *Opt*$^{-/-}$ phenotype was its acute onset, progressing from a developmentally delayed but intact skeleton at birth to severely impaired bone formation and widespread fractures by P10. Coincident with skeletal degeneration, we uncovered an abrupt failure of osteoblast maturation in vivo as indicated by a rapid decline in serum osteocalcin and bone *Ocn* expression. Similarly, type I collagen synthesis in cultured *Opt*$^{-/-}$ osteoblasts dropped significantly during the transition from a proliferative to a differentiating state. In contrast, osteocyte gene expression was up-regulated in mutant bones, suggesting that immature osteoblasts lacking Opt may bypass the normal differentiation program and instead undergo premature terminal differentiation to less metabolically active osteocytes. Loss of Opt did not alter the expression of transcription factors that drive commitment to the osteoblast lineage, which is consistent with a requirement for Opt in the maturation of committed osteoblasts. A second notable feature of the *Opt*$^{-/-}$ phenotype was the restriction of overt consequences of Opt deficiency to endochondral and membranous bone. This apparent specificity may reflect the importance of Opt for type I collagen synthesis, as type I collagen is the major protein synthesized by osteoblasts and constitutes ~90% of the organic bone matrix (Young, 2003). In this respect, our finding that primary differentiating *Opt*$^{-/-}$ osteoblasts synthesize and secrete reduced amounts of overmodified collagen chains supports the conclusion that Opt in osteoblasts is essential for proper type I collagen synthesis and/or processing. Compromised collagen synthesis in turn may explain the acute onset of low bone mass and fractures in perinatal *Opt*$^{-/-}$ mice undergoing robust bone formation and rapid growth.

Consistent with in vivo results, cultured *Opt*$^{-/-}$ osteoblasts synthesized a sparse collagen matrix and formed less-mineralized bone than WT osteoblasts. However, unlike the situation in vivo, *Col1a1* and *Col1a2* mRNA expression was not significantly decreased in primary osteoblasts from mutant mice. Together with the smaller size of *Opt*$^{-/-}$ osteoblasts in vivo, these data suggested a posttranscriptional defect in type I collagen synthesis that was confirmed by metabolic labeling. Based on these results, we hypothesize that during late embryonic and early postnatal development, suboptimal synthesis of potentially overmodified type I collagen by *Opt*$^{-/-}$ osteoblasts, coupled with ongoing osteoclastic resorption, produces an inadequate matrix that limits osteoblast differentiation, as reflected by decreased expression of osteoblast marker genes, including *Col1a1*/*Col1a2* and *Ocn* (Fig. 9; Aronow et al., 1990; Andrianarivo et al., 1992; Lynch et al., 1995). Impaired osteoblast differentiation

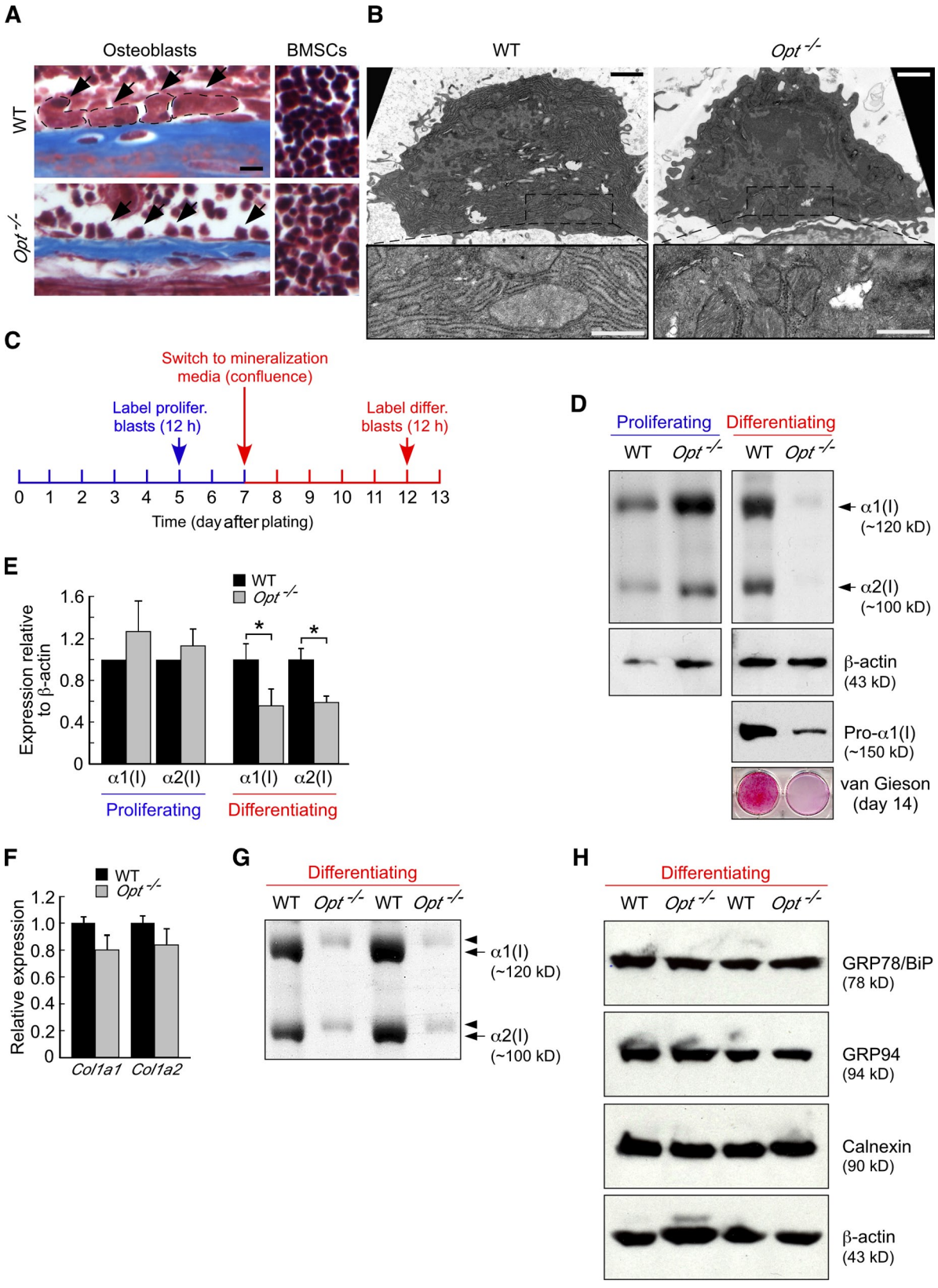

Figure 7. **Opt is essential for type I collagen synthesis in differentiating osteoblasts.** (A) Masson's trichrome staining of P10 tibial sections. Arrows indicate osteoblasts lining the endosteal bone surface (left), and WT osteoblasts are delineated by the dashed lines. *Opt*$^{-/-}$ osteoblasts are considerably smaller, whereas bone marrow stromal cells (BMSCs; right) are similar in size to WT. Bar, 10 µm. (B) Transmission electron microscopy of osteoblasts in P10 tibiae. (bottom) Higher magnification views of boxed regions show extensive, well-organized rER cisternae in WT that are absent in the more fibroblast-like *Opt*$^{-/-}$ cell. Bars: (top) 1 µm; (bottom) 0.5 µm. (C) Schematic timeline for metabolic labeling of osteoblasts. (D) 7% SDS-PAGE analysis of type I collagen synthesis by [^{3}H]proline-labeled proliferating and differentiating osteoblast cultures (top). Radiolabeled collagen from the media fraction is shown, with loading

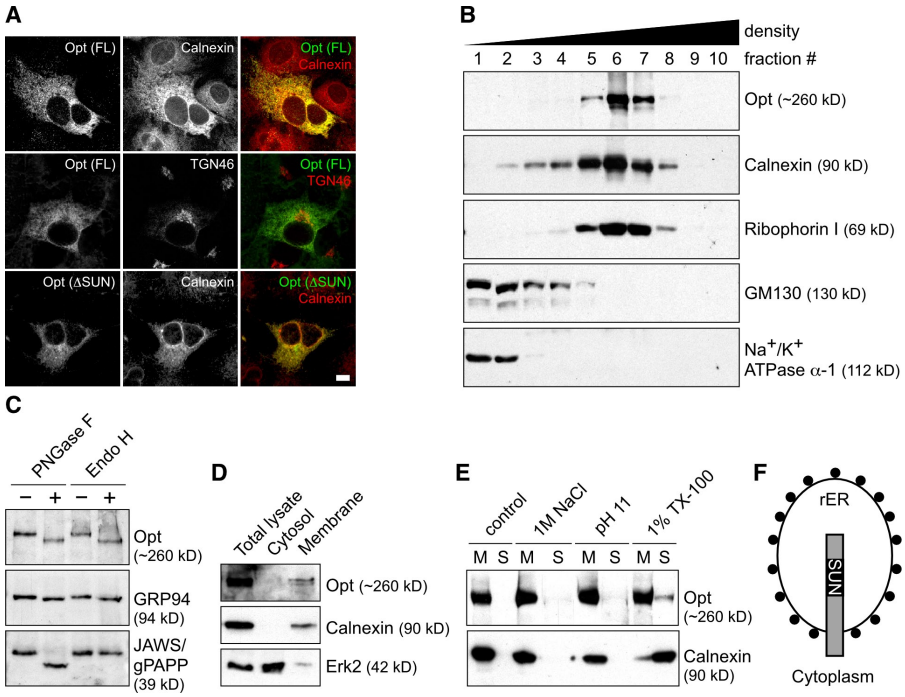

Figure 8. **Opt is a glycosylated integral membrane protein of the rER.** (A) Indirect immunofluorescence of HA-tagged full-length (FL) and SUN domain–deleted (ΔSUN) Opt in transfected primary osteoblasts. Antibodies against calnexin and TGN46 were used to label the ER and Golgi, respectively. Bar, 10 µm. (B) Subcellular fractionation of mouse embryonic fibroblast lysate on a continuous (0–20%) iodixanol density gradient. 10 fractions were collected and analyzed by SDS-PAGE and immunoblotting. Ribophorin I, GM130, and Na^+/K^+ ATPase-α1 mark the rER, Golgi, and plasma membrane, respectively. (C) Opt is N-glycosylated. Denatured lysate was treated with buffer (−) or with the N-glycosidases PNGase F or Endo H (+), and samples were immunoblotted for Opt, the Endo H–sensitive ER glycoprotein GRP94, or the Endo H–resistant Golgi glycoprotein JAWS/gPAPP. (D) Cytosolic and membrane fractions were immunoblotted for the indicated proteins. (E) Membrane fractions were treated with buffer ± 1 M NaCl, 0.1 M Na_2CO_3, pH 11, or 1% Triton X-100 and recentrifuged. The resulting membrane (M) and soluble (S) fractions were immunoblotted for Opt or calnexin, an ER-integral membrane protein. (F) Diagram showing the proposed orientation of Opt in the rER membrane, with the SUN domain on the lumenal side. Black circles represent ribosomes.

would then exacerbate the skeletal phenotype by further diminishing collagen synthesis and matrix deposition, culminating in brittle bones. The discrepancy between our in vivo and ex vivo *Col1a1*/*Col1a2* expression data remains to be resolved but may reflect complex regulatory mechanisms that are uncoupled in primary $Opt^{-/-}$ cultures (Lian and Stein, 1992). For example, mature osteoblasts can influence the differentiation potential of immature osteoblasts in vivo (Wang et al., 2007; Mak et al., 2008), raising the possibility that the acute loss of mature osteoblasts in $Opt^{-/-}$ mice secondarily impairs the differentiation of immature *Col1a1*/*Col1a2*-expressing cells. Supporting this model (Fig. 9), analyses of fracture calluses in $Opt^{-/-}$ mice revealed robust *Col1a1* expression in the absence of *Ocn* expression and appreciable bone formation, suggesting that decreased *Col1a1*/*Col1a2* expression in intact P10 bones is a secondary consequence of reduced matrix deposition.

Our data do not exclude that Opt may have other cell-autonomous roles unrelated to collagen production during osteoblast maturation or that additional noncell-autonomous mechanisms may contribute to the skeletal defects of $Opt^{-/-}$ mice. Consistent with these possibilities, plating primary $Opt^{-/-}$ osteoblasts on type I collagen failed to restore WT bone formation (Fig. S3 B). Nonetheless, the combined effect of reducing collagen translation and ultimately transcription in postnatal long bones subjected to load-bearing stresses provides a compelling explanation for the increased incidence of spontaneous fractures throughout the $Opt^{-/-}$ appendicular and axial skeleton.

The disruption of rER ultrastructure in vivo and the production of overmodified collagen chains ex vivo suggested that the rER is defective in osteoblasts lacking Opt, an rER integral membrane protein. Specifically, decreased production of overmodified collagen by $Opt^{-/-}$ osteoblasts implies that Opt may be an essential component of the osteoblast protein synthesis and processing machinery that couples robust collagen synthesis to maximal rER expansion. In this regard, a recent quantitative screen in *Saccharomyces cerevisiae* for gene deletions that disrupt ER protein folding identified Slp1, the budding yeast orthologue of Opt (Jonikas et al. 2009); however, a precise biochemical function for Slp1 remains elusive. Alternatively, given that the ER and outer nuclear membrane form a contiguous network, Opt may ensure rER integrity through binding of its SUN domain to one or more unidentified KASH domain proteins in the nuclear or rER membrane (Tzur et al., 2006; Ding et al., 2007; King et al., 2008; Chi et al., 2009; Razafsky and Hodzic, 2009). In this way, Opt may ensure rER membrane integrity and thus responsiveness to increased metabolic demand, a hypothesis supported by our ultrastructural analyses showing a sparsely organized rER in $Opt^{-/-}$ osteoblasts. Loss

normalized by sample volume rather than cell number. β-Actin and intracellular procollagen levels were assessed by immunoblotting, whereas van Gieson staining (bottom) confirms the sparse collagen matrix deposited by $Opt^{-/-}$ osteoblasts. (E) Quantification of type I collagen synthesis (α1 and α2 chains) by proliferating and differentiating osteoblasts normalized to β-actin control ($n = 4$ independent experiments in triplicate). *, $P < 0.02$. (F) qRT-PCR analysis of *Col1a1* and *Col1a2* expression in differentiating osteoblasts. (G) Overmodification of radiolabeled α1(I) and α2(I) collagen chains from differentiating $Opt^{-/-}$ osteoblasts, as indicated by their delayed electrophoretic migration. The autoradiogram shows radiolabeled collagen from the cellular fraction of duplicate cultures and represents an independent experiment from that shown in D. (H) Immunoblotting for the ER chaperones GRP78/BiP, GRP94, and calnexin in whole cell lysates of metabolically labeled, primary differentiating osteoblasts. β-Actin serves as a loading control. Results from two independent experiments are shown. Error bars indicate SEM.

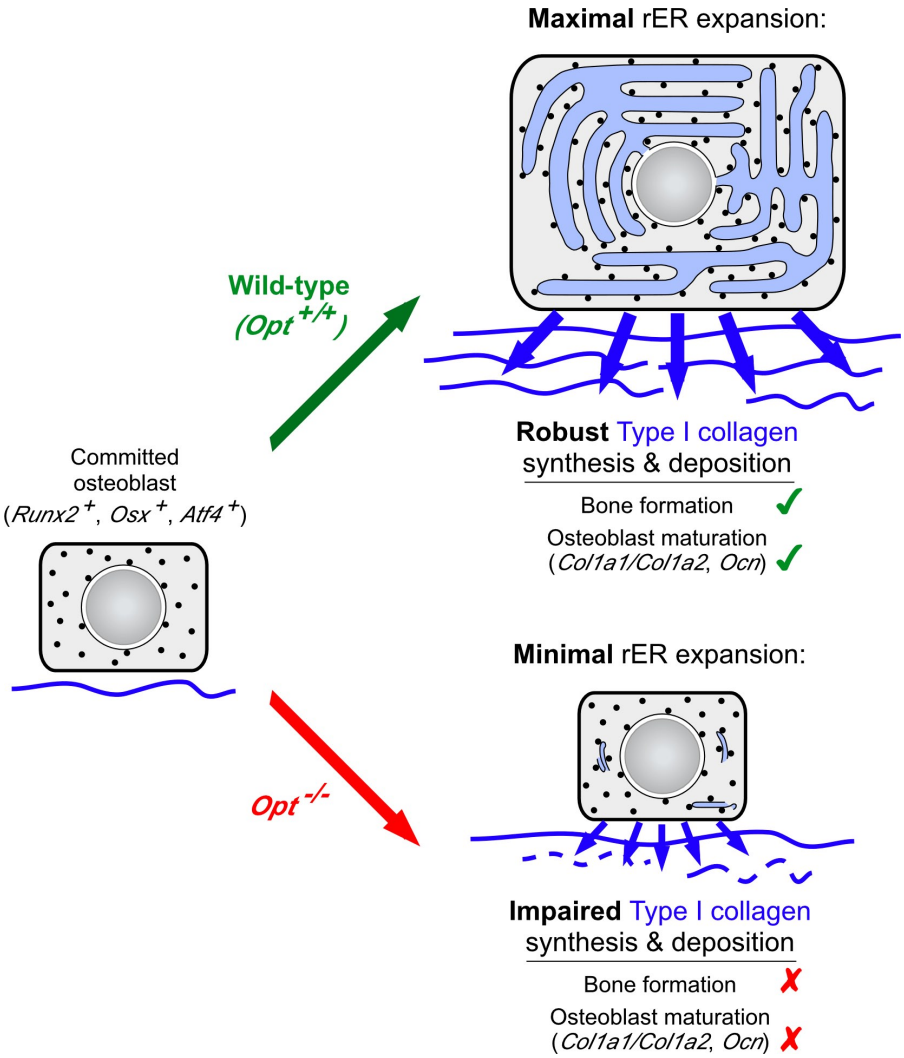

Figure 9. **Model for the Opt-dependent control of osteoblast function and bone formation.** Opt at the rER membrane promotes bone formation by enabling maximal rER expansion and robust type I collagen synthesis. Collagen matrix deposition in turn potentiates osteoblast maturation, leading to bone mass accrual. Black circles represent ribosomes.

of rER integrity in turn may reduce the efficiency of collagen synthesis and processing, leading to the decreased synthesis of overmodified collagen. Together with these possibilities and analogous to nuclear membrane–localized SUN domain proteins, Opt may act as a biomechanical adaptor protein that connects the rER lumen to the cytoskeleton, positioning and stabilizing the rER within the cell and enabling communication between distinct intracellular environments. The relative resistance of membrane-bound Opt to detergent solubilization is consistent with such an association. These possibilities are not mutually exclusive but provide testable hypotheses for how the metabolically active osteoblast couples type I collagen synthesis to rER expansion.

The short stature and skeletal defects of $Opt^{-/-}$ mice strongly resemble those of patients having severe or lethal forms of OI. Classical OI is caused by mutations in either of the two genes encoding type I collagen (Byers and Cole, 2002); however, a spectrum of distinct clinical subtypes not linked to *Col1a1* or *Col1a2* has also been reported (Aitchison et al., 1988; Williams et al., 1989; Wallis et al., 1993; Glorieux et al., 2002; Ward et al., 2002). In particular, hyperplastic callus formation and abnormal bone lamellation are hallmarks of both the $Opt^{-/-}$ phenotype and OI type V (Glorieux et al., 2000). Although mutations in the genes encoding the collagen-modifying proteins, cartilage-associated protein and prolyl 3-hydroxylase 1, have been identified in several patients (Morello et al., 2006; Cabral et al., 2007), the genetic etiology of other diverse subtypes including OI type V is not known. We speculate that loss of function mutations in human *Opt* may underlie one or more noncollagen OI subtypes, although initial experiments to test this hypothesis identified no significant change in *Opt* transcript or protein levels in fibroblasts from four OI type V probands. Likewise, mutations in *Opt* may contribute to fibrogenesis imperfecta ossium, a rare bone disorder of unknown etiology, which, like the *Opt* phenotype, manifests with fractures, abnormal collagen birefringence, and elevated serum ALP (Baker, 1956; Sissons, 2000). Finally, several major quantitative trait loci for bone mineral density map to the region of chromosome 1 containing the *Opt* locus (Xiong et al., 2009). Thus, our data implicate human *Opt* as a novel candidate gene for OI and other disorders of low bone mass. Further study of how Opt influences ER dynamics and promotes type I collagen synthesis will be instrumental in better understanding the brittle bone phenotype that results from Opt deficiency.

Materials and methods

Mouse strains

The KST50 mouse embryonic stem cell line, containing an insertion of the pGT0TMpf gene trap vector in the *Opt* locus, was isolated and characterized as described previously (Mitchell et al., 2001). *Opt* F1 heterozygotes were backcrossed to C57BL/6 mice for at least six generations before intercrossing. Genotyping was performed by X-gal staining of yolk sacs and/or tail biopsies or by RT-PCR using primers flanking the insertion site (forward, 5′-TTCTAATGGAGGTCCACATGC-3′; *Opt*-specific reverse, 5′-TGACGTTCTGACTGATACTGGG-3′; gene trap vector–specific reverse, 5′-GAGACCTGGGGTATCTGAAGG-3′). All animal experiments were approved by the University of California Berkeley Institutional Animal Care and Use Committee.

Morphological analysis, histology, and in situ hybridization

Alcian blue and Alizarin red staining of skeletal preparations, X-gal staining, and radioactive in situ hybridization with ^{35}S-labeled riboprobes were performed according to established protocols (Nagy, 2003). To assess 3D trabecular and 2D cortical structural parameters, the distal femur and proximal tibia from 10-d-old mice were measured directly as described previously (Jiang et al., 2005) using a desktop μCT 40 with an isotropic resolution of 12 μm in all three spatial dimensions (SCANCO Medical). For histological analysis of collagen matrix, deparaffinized 6-μm sections were stained by Masson's trichrome and counterstained with Weigert's iron hematoxylin (Sigma-Aldrich). Alternatively, collagen fibers were stained with Sirius red F3B/Direct red 80 (Sigma-Aldrich) for polarization microscopy. Undecalcified sections from methylmethacrylate-embedded femurs were stained by Goldner's trichrome to distinguish osteoid from mineralized bone. Fracture calluses were visualized by staining with 0.02% aqueous Fast green (Sigma-Aldrich) followed by rinsing in 1% acetic acid and staining in 0.1% Safranin O (Sigma-Aldrich). Cell proliferation and apoptosis were quantified in deparaffinized 6-μm serial sections of P3 hindlimbs using a PCNA staining kit (Invitrogen) and In situ Cell Death Detection kit (Roche), respectively. TRAP activity was visualized histochemically using the Leukocyte Acid Phosphatase kit (Sigma-Aldrich). Sections were viewed with a microscope (Axioplan; Carl Zeiss, Inc.) equipped with Plan Neofluar objectives (10× 0.3 NA, 20× 0.5 NA, and 40× 0.75 NA) and Chroma optical filters (41001 FITC, 41004 Texas red, and 31000 DAPI/Hoechst), and images were captured using a digital camera (DFC500; Leica). To enhance contrast against the Hoechst counterstain, radioactive in situ signals were photographed in brightfield and pseudocolored red using the Colorize option within the Hue/Saturation command in Photoshop (version 7.0; Adobe).

Bioinformatics, antibodies, and expression experiments

Opt transcripts were detected by Northern blotting of TRIzol-extracted total RNA probed with a ^{32}P-labeled cDNA fragment spanning nucleotides 4,399–5,120 of the *Opt* mRNA (Mouse Genome Informatics no. AI848100; GenBank accession no. NM_172645.2). Alternatively, total RNA was purified using the RNeasy MinElute Cleanup kit (QIAGEN), and mRNA expression was assessed by qRT-PCR with SYBR green reagents on a system (7300; Applied Biosystems) using β-tubulin as an internal reference. Primer sequences are provided in Table S1. For heterologous expression, the full-length Opt open reading frame (OptFL) was PCR amplified from WT femur cDNA and subcloned into a modified pcDNA3 vector (Invitrogen) containing a C-terminal HA epitope tag. An Opt fragment lacking the SUN domain was generated by overlap PCR and substituted for the BstXI–EcoRI fragment of OptFL to generate the OptΔSUN construct. All constructs were verified by sequencing. For Opt immunoblotting, a rabbit polyclonal antibody was raised and affinity purified against the peptide N-CQKTKTEKRALKRRRSK-C corresponding to an epitope in the Opt cytosolic domain (Covance). Other primary antibodies were rabbit type I collagen (AB765P; Millipore), rabbit actin C-11 (Santa Cruz Biotechnology, Inc.), mouse HA tag HA-7 (Sigma-Aldrich), rabbit calnexin (C4731; Sigma-Aldrich), rabbit Erk2 C-14 (Santa Cruz Biotechnology, Inc.), mouse GM130 (BD), and mouse Na^+/K^+ ATPase α-1 C464.6 (Millipore).

Primary cell cultures and metabolic labeling

Mouse embryonic fibroblasts were isolated from E13.5 embryos according to established protocols, maintained in high glucose DME (Invitrogen) with 10% FBS (HyClone) and antibiotics, and used after no more than five passages. Primary calvarial osteoblasts were isolated from 4- to 8-d-old mice by five sequential digestions in PBS containing 0.1% collagenase P (Roche) and 0.05% trypsin EDTA (Invitrogen). Cells from digestions 2–5 were pooled, plated at 12,000 cells/cm^2 in 6-well plates, grown to confluence in αMEM/10% FBS with antibiotics, and differentiated in media containing 100 μg/ml ascorbate and 5 mM β-glycerophosphate. For the experiments shown in Fig. S3, osteoblasts were plated in collagen I 6-well multiwell plates (BD). For histochemical assessment of ALP activity, osteoblast cultures were fixed in 4% paraformaldehyde and stained for 20 min with a solution containing 0.1 mg/ml naphthol AS-MX phosphate and 0.6 mg/ml Fast blue BB salt (Sigma-Aldrich). To visualize the collagen matrix, cell cultures were fixed in 4% paraformaldehyde, stained for 10 min with van Gieson reagent (prepared as 10 ml 1% acid fuchsin in 100 ml saturated aqueous picric acid), rinsed twice with 70% ethanol, and dehydrated to 100% ethanol.

For mineralization assays, cultures were fixed in 4% paraformaldehyde, stained for 30 min with 0.1% Alizarin red, pH 5.5, and rinsed several times with deionized water to remove nonspecifically bound stain. The retained Alizarin red was eluted with 10% cetylpyridinium chloride and quantified spectrophotometrically at 562 nm relative to known calcium standards. ALP-, van Gieson–, and Alizarin red–stained osteoblast cultures were imaged on a flatbed scanner (Perfection 2450; Epson). For determination of cell number, cultures were fixed in 4% paraformaldehyde, permeabilized with 20% methanol, stained for 30 min with 0.5% crystal violet (Sigma-Aldrich) in 20% methanol, and rinsed three times with deionized water to remove nonspecifically bound stain. The retained crystal violet was eluted with 10% acetic acid and quantified spectrophotometrically at 595 nm. Cell proliferation in primary osteoblasts was measured by a BrdU cell proliferation assay (EMD). Collagen synthesis was assessed by metabolic labeling as described previously (Yang et al., 2004; Yu et al., 2005). In brief, proliferating or differentiating osteoblasts were labeled for 12 h with 50 μCi/ml [^{3}H]proline (GE Healthcare) in αMEM supplemented with 2% dialyzed FBS and 2 mM GlutaMAX (Invitrogen). Osteoblasts were harvested by scraping into 500 μl ice-cold PBS with protease inhibitors (Roche), and a 200-μl fraction was reserved for β-actin and procollagen-α1(I) immunoblotting. Procollagen from the medium and cell layers was digested to collagen with 50 μg/ml pepsin in 0.5 M acetic acid for 24 h at 4°C, precipitated with 0.7 M NaCl, and resolved by SDS-PAGE on a 7% gel containing 2 M urea. Gels were impregnated with fluorographic reagent (Amplify; GE Healthcare), dried, and exposed to BioMax MS film (Kodak). Type I collagen signal intensity was quantified using the ImageJ software (version1.40g; National Institutes of Health) and normalized to β-actin protein expression.

Transmission electron microscopy and confocal imaging

After initial fixation by intracardial perfusion, dissected tibiae and pancreas were fixed at 4°C in 2% paraformaldehyde/2% glutaraldehyde/0.1 M sodium cacodylate, pH 7.35. To decalcify tibiae from P10 mice, 0.1 M EDTA was included in the fixative, and samples were nutated gently for 10–14 d at 4°C. Samples were washed to remove excess EDTA, postfixed in 1% osmium tetroxide, dehydrated, and embedded in epon (epoxy) resin (Hayat, 2000). Ultrathin sections of 80 nm were stained with uranyl acetate and viewed with a transmission electron microscope (Philips CM120; FEI Company), and images were captured with a digital camera (BioScan; Gatan). Osteoblasts were identified by their morphology and proximity to the bone matrix. For indirect immunofluorescence, cells grown on 24-well glass coverslips were transfected with 250 ng OptFL or OptΔSUN using Lipofectamine 2000 reagent (Invitrogen), fixed and permeabilized in methanol/acetone 40–48 h later, blocked in 5% goat serum, immunostained with primary antibodies overnight, and visualized with Alexa Fluor 488– and 555–conjugated secondary antibodies (Invitrogen). Coverslips were mounted in mounting medium (Vectashield HardSet; Vector Laboratories) and stored in the dark at 4°C. Confocal imaging was performed with a microscope (DM RE; Leica) using a 63× 1.4 NA oil immersion objective lens and TCS software (version 2.61; Leica). Images were processed for brightness and contrast using Photoshop (version 7.0).

Subcellular fractionation

Membrane and cytosolic fractions were prepared by a standard ultracentrifugation protocol. For subcellular fractionation, mouse embryonic fibroblasts (~5 × 10^7) were resuspended in ice-cold homogenization buffer (0.25 M sucrose in 10 mM Hepes, pH 7.4, and 1 mM EDTA) and disrupted gently by 30 strokes in a prechilled Wheaton dounce homogenizer followed by five passages through a 22-gauge needle. After a 10-min centrifugation step at 2,000 *g*, the postnuclear supernatant was layered atop a continuous 0–20% iodixanol (OptiPrep; Sigma-Aldrich) density gradient prepared in homogenization buffer. Gradients were centrifuged at 34,100 rpm for 3.25 h at 4°C in a rotor (SW41Ti; Beckman Coulter), and 10 fractions were collected from the top of the tube. Gradient integrity was

confirmed using an Abbe refractometer. Proteins were precipitated in 10% trichloroacetic acid, washed with ice-cold acetone, and analyzed by SDS-PAGE and immunoblotting using Western Lightning Plus-ECL substrate (PerkinElmer) for signal detection. Similar results were obtained by discontinuous sucrose density gradient ultracentrifugation.

Clinical biochemistry

Serum and urine parameters were quantified by ELISA using commercially available kits for mouse osteocalcin (Biomedical Technologies), IGF-1 (Diagnostic Systems Laboratories), parathyroid hormone (Immutopics), osteoclast-specific TRAP 5b (Immunodiagnostic Systems), insulin (Crystal Chem), and total urinary deoxypyridinoline (Quidel). Ascorbic acid (BioVision) and urinary creatinine (Quidel) were quantified by colorimetric assay. Calcium, phosphate, ALP, and glucose were measured by the Comparative Pathology Laboratory at the University of California (Davis, Davis, CA).

Statistical analysis

Data are expressed as mean ± SEM. Student's *t* test and analysis of variance with Tukey's Honestly Significant Difference post hoc test were used to calculate statistical significance for two and three samples, respectively. Statistical analysis was performed using Kaleidagraph (version 4.0; Synergy Software), and values were considered significant at $P < 0.05$.

Online supplemental material

Fig. S1 shows developmentally delayed but intact skeletal elements from newborn *Opt*$^{-/-}$ mice. Fig. S2 shows chondrocyte and osteoblast differentiation markers in E14.5 and E17.5 embryos, respectively, and representative transmission electron microscopy images of osteoblasts from E17.5 embryos. Fig. S3 shows that plating *Opt*$^{-/-}$ osteoblasts on type I collagen neither normalizes bone formation nor reveals any defects in cell matrix adhesion. Fig. S4 shows that Opt deficiency does not affect pancreatic function or morphology. Table S1 provides sequences for qRT-PCR primers used in this study. Online supplemental material is available at http://www.jcb.org/cgi/content/full/jcb.201003006/DC1.

We thank David Stafford, Jen-Yi Lee, and Tamara Alliston for critical reading of the manuscript; J-Y.L. for confocal imaging expertise; Edivinia Pangilinan for mouse husbandry; Haitao Li, Ken Campellone, Chris Fromme, and Bertrand Kleizen for expertise and advice and for TGN46 (K. Campellone) and ribophorin I (C. Fromme) antibodies; David Eyre and MaryAnn Weis for mass spectrometry analyses; Joan Marini and Pierre Moffatt for OI case diagnosis and proband fibroblast samples; Jane Yu for technical assistance; Benjamin Boudignon for histomorphometry; Grete Adamson, Patricia Kysar, and Khushdeep Kaur (Electron Microscopy Laboratory, University of California [UC], Davis) for technical assistance and expertise with TEM; Marian Derby and Philippe Labelle (Comparative Pathology Laboratory, UC, Davis) for technical assistance with clinical chemistry and for expertise with animal necropsy, respectively; Gerard Karsenty for in situ hybridization probes; Christopher Nicchitta for GRP78/BiP and GRP94 antisera; Venice Calinisan for Erk2 antibody; Pedro Gutierrez for amylase, glucagon, and insulin antibodies; Millan Patel and Vionnie Yu for helpful discussions; and Kathy Pinson and Bill Skarnes for expertise in the initial stages of the project.

M.L. Sohaskey was a Michael Geisman Fellow of the Osteogenesis Imperfecta Foundation and a Foundation for Advanced Cancer Studies and Merck Fellow of the Life Sciences Research Foundation. This work was supported by National Institutes of Health (grant GM49346 to R.M. Harland).

Submitted: 1 March 2010
Accepted: 12 April 2010

References

Aitchison, K., D. Ogilvie, M. Honeyman, E. Thompson, and B. Sykes. 1988. Homozygous osteogenesis imperfecta unlinked to collagen I genes. *Hum. Genet.* 78:233–236. doi:10.1007/BF00291667

Andrianarivo, A.G., J.A. Robinson, K.G. Mann, and R.P. Tracy. 1992. Growth on type I collagen promotes expression of the osteoblastic phenotype in human osteosarcoma MG-63 cells. *J. Cell. Physiol.* 153:256–265. doi:10.1002/jcp.1041530205

Aronow, M.A., L.C. Gerstenfeld, T.A. Owen, M.S. Tassinari, G.S. Stein, and J.B. Lian. 1990. Factors that promote progressive development of the osteoblast phenotype in cultured fetal rat calvaria cells. *J. Cell. Physiol.* 143:213–221. doi:10.1002/jcp.1041430203

Baker, S.L. 1956. Fibrogenesis imperfecta ossium; a generalised disease of bone characterised by defective formation of the collagen fibres of the bone matrix. *J. Bone Joint Surg. Br.* 38-B:378–417.

Baker, J., J.P. Liu, E.J. Robertson, and A. Efstratiadis. 1993. Role of insulin-like growth factors in embryonic and postnatal growth. *Cell.* 75:73–82.

Behonick, D.J., Z. Xing, S. Lieu, J.M. Buckley, J.C. Lotz, R.S. Marcucio, Z. Werb, T. Miclau, and C. Colnot. 2007. Role of matrix metalloproteinase 13 in both endochondral and intramembranous ossification during skeletal regeneration. *PLoS One.* 2:e1150. doi:10.1371/journal.pone.0001150

Boyle, W.J., W.S. Simonet, and D.L. Lacey. 2003. Osteoclast differentiation and activation. *Nature.* 423:337–342. doi:10.1038/nature01658

Byers, P.H., and W.G. Cole. 2002. Osteogenesis imperfecta. *In* Connective Tissue and Its Heritable Disorders: Molecular, Genetical, and Medical Aspects. Second edition. P.M. Royce and B. Steinmann, editors. Wiley-Liss, Inc., New York. 385–430.

Cabral, W.A., W. Chang, A.M. Barnes, M. Weis, M.A. Scott, S. Leikin, E. Makareeva, N.V. Kuznetsova, K.N. Rosenbaum, C.J. Tifft, et al. 2007. Prolyl 3-hydroxylase 1 deficiency causes a recessive metabolic bone disorder resembling lethal/severe osteogenesis imperfecta. *Nat. Genet.* 39:359–365. doi:10.1038/ng1968

Chi, Y.H., L.I. Cheng, T. Myers, J.M. Ward, E. Williams, Q. Su, L. Faucette, J.Y. Wang, and K.T. Jeang. 2009. Requirement for Sun1 in the expression of meiotic reproductive genes and piRNA. *Development.* 136:965–973. doi:10.1242/dev.029868

Colnot, C., Z. Thompson, T. Miclau, Z. Werb, and J.A. Helms. 2003. Altered fracture repair in the absence of MMP9. *Development.* 130:4123–4133. doi:10.1242/dev.00559

Ding, X., R. Xu, J. Yu, T. Xu, Y. Zhuang, and M. Han. 2007. SUN1 is required for telomere attachment to nuclear envelope and gametogenesis in mice. *Dev. Cell.* 12:863–872. doi:10.1016/j.devcel.2007.03.018

Ferguson, C., E. Alpern, T. Miclau, and J.A. Helms. 1999. Does adult fracture repair recapitulate embryonic skeletal formation? *Mech. Dev.* 87:57–66. doi:10.1016/S0925-4773(99)00142-2

Frederick, J.P., A.T. Tafari, S.M. Wu, L.C. Megosh, S.T. Chiou, R.P. Irving, and J.D. York. 2008. A role for a lithium-inhibited Golgi nucleotidase in skeletal development and sulfation. *Proc. Natl. Acad. Sci. USA.* 105:11605–11612. doi:10.1073/pnas.0801182105

Glorieux, F.H., F. Rauch, H. Plotkin, L. Ward, R. Travers, P. Roughley, L. Lalic, D.F. Glorieux, F. Fassier, and N.J. Bishop. 2000. Type V osteogenesis imperfecta: a new form of brittle bone disease. *J. Bone Miner. Res.* 15:1650–1658. doi:10.1359/jbmr.2000.15.9.1650

Glorieux, F.H., L.M. Ward, F. Rauch, L. Lalic, P.J. Roughley, and R. Travers. 2002. Osteogenesis imperfecta type VI: a form of brittle bone disease with a mineralization defect. *J. Bone Miner. Res.* 17:30–38. doi:10.1359/jbmr.2002.17.1.30

Hayat, M.A. 2000. Principles and Techniques of Electron Microscopy: Biological Applications. Fourth edition. Cambridge University Press, Cambridge/New York. 543 pp.

Hernandez, C.J., R.J. Majeska, and M.B. Schaffler. 2004. Osteocyte density in woven bone. *Bone.* 35:1095–1099. doi:10.1016/j.bone.2004.07.002

Hsiao, E.C., B.M. Boudignon, W.C. Chang, M. Bencsik, J. Peng, T.D. Nguyen, C. Manalac, B.P. Halloran, B.R. Conklin, and R.A. Nissenson. 2008. Osteoblast expression of an engineered Gs-coupled receptor dramatically increases bone mass. *Proc. Natl. Acad. Sci. USA.* 105:1209–1214. doi:10.1073/pnas.0707457105

Jiang, Y., J. Zhao, E.Y. Liao, R.C. Dai, X.P. Wu, and H.K. Genant. 2005. Application of micro-CT assessment of 3-D bone microstructure in preclinical and clinical studies. *J. Bone Miner. Metab.* 23(Suppl):122–131. doi:10.1007/BF03026336

Jilka, R.L., R.S. Weinstein, T. Bellido, P. Roberson, A.M. Parfitt, and S.C. Manolagas. 1999. Increased bone formation by prevention of osteoblast apoptosis with parathyroid hormone. *J. Clin. Invest.* 104:439–446. doi:10.1172/JCI6610

Jonikas, M.C., S.R. Collins, V. Denic, E. Oh, E.M. Quan, V. Schmid, J. Weibezahn, B. Schwappach, P. Walter, J.S. Weissman, and M. Schuldiner. 2009. Comprehensive characterization of genes required for protein folding in the endoplasmic reticulum. *Science.* 323:1693–1697. doi:10.1126/science.1167983

Karsenty, G. 2008. Transcriptional control of skeletogenesis. *Annu. Rev. Genomics Hum. Genet.* 9:183–196. doi:10.1146/annurev.genom.9.081307.164437

Karsenty, G., and E.F. Wagner. 2002. Reaching a genetic and molecular understanding of skeletal development. *Dev. Cell.* 2:389–406. doi:10.1016/S1534-5807(02)00157-0

King, M.C., T.G. Drivas, and G. Blobel. 2008. A network of nuclear envelope membrane proteins linking centromeres to microtubules. *Cell.* 134:427–438. doi:10.1016/j.cell.2008.06.022

Kreibich, G., B.L. Ulrich, and D.D. Sabatini. 1978. Proteins of rough microsomal membranes related to ribosome binding. I. Identification of ribophorins I and II, membrane proteins characteristics of rough microsomes. *J. Cell Biol.* 77:464–487. doi:10.1083/jcb.77.2.464

Lamandé, S.R., and J.F. Bateman. 1999. Procollagen folding and assembly: the role of endoplasmic reticulum enzymes and molecular chaperones. *Semin. Cell Dev. Biol.* 10:455–464. doi:10.1006/scdb.1999.0317

Lian, J.B., and G.S. Stein. 1992. Concepts of osteoblast growth and differentiation: basis for modulation of bone cell development and tissue formation. *Crit. Rev. Oral Biol. Med.* 3:269–305.

Lynch, M.P., J.L. Stein, G.S. Stein, and J.B. Lian. 1995. The influence of type I collagen on the development and maintenance of the osteoblast phenotype in primary and passaged rat calvarial osteoblasts: modification of expression of genes supporting cell growth, adhesion, and extracellular matrix mineralization. *Exp. Cell Res.* 216:35–45. doi:10.1006/excr.1995.1005

Mak, K.K., H.M. Kronenberg, P.T. Chuang, S. Mackem, and Y. Yang. 2008. Indian hedgehog signals independently of PTHrP to promote chondrocyte hypertrophy. *Development.* 135:1947–1956. doi:10.1242/dev.018044

Mitchell, K.J., K.I. Pinson, O.G. Kelly, J. Brennan, J. Zupicich, P. Scherz, P.A. Leighton, L.V. Goodrich, X. Lu, B.J. Avery, et al. 2001. Functional analysis of secreted and transmembrane proteins critical to mouse development. *Nat. Genet.* 28:241–249. doi:10.1038/90074

Mohan, S., A. Kapoor, A. Singgih, Z. Zhang, T. Taylor, H. Yu, R.B. Chadwick, Y.S. Chung, Y.S. Chung, L.R. Donahue, et al. 2005. Spontaneous fractures in the mouse mutant sfx are caused by deletion of the gulonolactone oxidase gene, causing vitamin C deficiency. *J. Bone Miner. Res.* 20:1597–1610. doi:10.1359/JBMR.050406

Morello, R., T.K. Bertin, Y. Chen, J. Hicks, L. Tonachini, M. Monticone, P. Castagnola, F. Rauch, F.H. Glorieux, J. Vranka, et al. 2006. CRTAP is required for prolyl 3- hydroxylation and mutations cause recessive osteogenesis imperfecta. *Cell.* 127:291–304. doi:10.1016/j.cell.2006.08.039

Myllyharju, J., and K.I. Kivirikko. 2004. Collagens, modifying enzymes and their mutations in humans, flies and worms. *Trends Genet.* 20:33–43. doi:10.1016/j.tig.2003.11.004

Nagy, A. 2003. Manipulating the Mouse Embryo: A Laboratory Manual. Third edition. Cold Spring Harbor Laboratory Press, Cold Spring Harbor, NY. 764 pp.

Noble, B.S., and J. Reeve. 2000. Osteocyte function, osteocyte death and bone fracture resistance. *Mol. Cell. Endocrinol.* 159:7–13. doi:10.1016/S0303-7207(99)00174-4

Razafsky, D., and D. Hodzic. 2009. Bringing KASH under the SUN: the many faces of nucleo-cytoskeletal connections. *J. Cell Biol.* 186:461–472. doi:10.1083/jcb.200906068

Rosen, C.J. 2004. Insulin-like growth factor I and bone mineral density: experience from animal models and human observational studies. *Best Pract. Res. Clin. Endocrinol. Metab.* 18:423–435. doi:10.1016/j.beem.2004.02.007

Sissons, H.A. 2000. Fibrogenesis imperfecta ossium (Baker's disease): a case studied at autopsy. *Bone.* 27:865–873. doi:10.1016/S8756-3282(00)00401-4

Skarnes, W.C., J.E. Moss, S.M. Hurtley, and R.S. Beddington. 1995. Capturing genes encoding membrane and secreted proteins important for mouse development. *Proc. Natl. Acad. Sci. USA.* 92:6592–6596. doi:10.1073/pnas.92.14.6592

Sohaskey, M.L., J. Yu, M.A. Diaz, A.H. Plaas, and R.M. Harland. 2008. JAWS coordinates chondrogenesis and synovial joint positioning. *Development.* 135:2215–2220. doi:10.1242/dev.019950

Thompson, Z., T. Miclau, D. Hu, and J.A. Helms. 2002. A model for intramembranous ossification during fracture healing. *J. Orthop. Res.* 20:1091–1098. doi:10.1016/S0736-0266(02)00017-7

Tzur, Y.B., K.L. Wilson, and Y. Gruenbaum. 2006. SUN-domain proteins: 'Velcro' that links the nucleoskeleton to the cytoskeleton. *Nat. Rev. Mol. Cell Biol.* 7:782–788. doi:10.1038/nrm2003

Vedrenne, C., and H.P. Hauri. 2006. Morphogenesis of the endoplasmic reticulum: beyond active membrane expansion. *Traffic.* 7:639–646. doi:10.1111/j.1600-0854.2006.00419.x

Wallis, G.A., B. Sykes, P.H. Byers, C.G. Mathew, D. Viljoen, and P. Beighton. 1993. Osteogenesis imperfecta type III: mutations in the type I collagen structural genes, COL1A1 and COL1A2, are not necessarily responsible. *J. Med. Genet.* 30:492–496. doi:10.1136/jmg.30.6.492

Wang, Y., S. Nishida, B.M. Boudignon, A. Burghardt, H.Z. Elalieh, M.M. Hamilton, S. Majumdar, B.P. Halloran, T.L. Clemens, and D.D. Bikle. 2007. IGF-I receptor is required for the anabolic actions of parathyroid hormone on bone. *J. Bone Miner. Res.* 22:1329–1337. doi:10.1359/jbmr.070517

Ward, L.M., F. Rauch, R. Travers, G. Chabot, E.M. Azouz, L. Lalic, P.J. Roughley, and F.H. Glorieux. 2002. Osteogenesis imperfecta type VII: an autosomal recessive form of brittle bone disease. *Bone.* 31:12–18. doi:10.1016/S8756-3282(02)00790-1

Williams, E.M., A.C. Nicholls, S.C. Daw, N. Mitchell, L.S. Levin, B. Green, J. MacKenzie, D.R. Evans, P.A. Chudleigh, and F.M. Pope. 1989. Phenotypical features of an unique Irish family with severe autosomal recessive osteogenesis imperfecta. *Clin. Genet.* 35:181–190.

Xiong, Q., Y. Jiao, K.A. Hasty, S.T. Canale, J.M. Stuart, W.G. Beamer, H.W. Deng, D. Baylink, and W. Gu. 2009. Quantitative trait loci, genes, and polymorphisms that regulate bone mineral density in mouse. *Genomics.* 93:401–414. doi:10.1016/j.ygeno.2008.12.008

Yang, X., K. Matsuda, P. Bialek, S. Jacquot, H.C. Masuoka, T. Schinke, L. Li, S. Brancorsini, P. Sassone-Corsi, T.M. Townes, et al. 2004. ATF4 is a substrate of RSK2 and an essential regulator of osteoblast biology; implication for Coffin-Lowry Syndrome. *Cell.* 117:387–398. doi:10.1016/S0092-8674(04)00344-7

Young, M.F. 2003. Bone matrix proteins: their function, regulation, and relationship to osteoporosis. *Osteoporos. Int.* 14(Suppl 3):S35–S42.

Yu, V.W., G. Ambartsoumian, L. Verlinden, J.M. Moir, J. Prud'homme, C. Gauthier, P.J. Roughley, and R. St-Arnaud. 2005. FIAT represses ATF4-mediated transcription to regulate bone mass in transgenic mice. *J. Cell Biol.* 169:591–601. doi:10.1083/jcb.200412139